

# Detection of Surface Waves During Femtosecond Filamentation

Travis Garrett,<sup>1</sup> Anna Janicek,<sup>1</sup> J. Todd Fayard II,<sup>2</sup> and Jennifer Elle<sup>1</sup>

<sup>1</sup>*Air Force Research Laboratory, Directed Energy Directorate, Albuquerque, NM 87123, USA*

<sup>2</sup>*Department of Physics and Astronomy, Mississippi State University, Mississippi State, MS 39762, USA*

Ultrashort pulsed lasers (USPL) can produce thin columns of plasma in air via femtosecond filamentation, and these plasmas have been found to generate broadband TeraHertz (THz) and Radio Frequency (RF) radiation. A recent theory argues that the currents driven at the boundary of the plasma excite a Surface Plasmon Polariton (SPP) surface wave (in particular a Sommerfeld-Goubau wave given the cylindrical symmetry), which proceeds to detach from the end of the plasma to become the RF pulse. We have performed near-field measurements of these plasmas with a D-dot probe, and find an excellent agreement with this theory. The radial field dependence is precisely fit by a Hankel function, with an outer length scale in agreement with plasma conductivity and radius, and a measured longitudinal drift in frequency maxima closely matches both SPP simulations and analytic expectations.

## INTRODUCTION

Surface waves can be excited across a spectrum of environments, including solitonic shallow water gravity waves [1–3], Rayleigh and Love surface acoustic waves (from microfluidic to planetary scale) [4–6], Dyakonov, Bloch, and Tamm electromagnetic surface waves along special dielectrics [7–11], and surface plasmon polaritons [12, 13] on the boundaries of conducting substrates with free electron number density  $n_e$ . Surface plasmon polaritons are composed of an electromagnetic wave coupled to a charge density wave on the boundary of the metal, semiconductor or plasma region, and can exist under a cut-off frequency  $\omega_s$ , which for a flat plane boundary equals  $\omega_s = \omega_{\text{pl}}/\sqrt{2}$ , where  $\omega_{\text{pl}}$  is the plasma frequency.

SPPs are typically considered along the boundaries of metals and semiconductors in the optical and infrared bands, where they can be driven by Otto or Kretschmann coupling [14, 15], but they can be excited along the boundary of a plasma as well. An Ultra Short Pulse Laser (USPL) can generate volumes of plasma in a unique way: given sufficient power Kerr self-focusing will boost the intensity of a standard 800nm, 50fs, Ti:Sapphire pulse propagating in air to roughly  $5 \times 10^{17}$  W/m<sup>2</sup>, at which point strong field ionization [16] creates a plasma of density roughly  $n_e \sim 10^{22}$  m<sup>-3</sup> and radius  $r_{\text{pl}} \sim 100$   $\mu\text{m}$ . USPL filamentation thus generates thin columns of plasma that grow longer at the speed of light [17–19], which have a wide array of potential applications [20–24].

In addition to creating the plasma, the femtosecond pulse also endows the plasma with initial current densities. A  $\mathbf{J} \times \mathbf{B}$  Lorentz force drives a direct longitudinal current density in the second half of the laser pulse ( $J_z$  for a pulse propagating in  $\hat{z}$ ), which is closely linked to broadband single color filament THz [25–28] (with an associated low frequency RF tail). Zhou et al [29] noted that transverse current densities ( $J_x$  for a linear  $\hat{x}$  polarized laser pulse, that evolves into  $J_r$  with collisions) are also generated by the laser pulse, and they argue that the resulting plasma wake trailing behind the laser pulse

will also excite RF radiation.

Stimulated by far field measurements of broadband RF from filamentation [30–34], several years ago our group developed a quantitative model of RF generation due to the transverse plasma currents [35]. Particle In Cell (PIC) simulations [36, 37] confirmed that a plasma wake is established on the outer boundary of the plasma; the magnitude of the associated  $J_r$  current is limited by electron neutral collisions at higher pressures, and by the build up of an electrostatic well at lower pressures (e.g. 1 Torr).

Larger scale continuum Drude simulations [38, 39] then lead to a surprise: the presence of the plasma wake current pulse  $J_r$  on the outer boundary of the plasma acts as an antenna and invariably excites a SPP (see also [40]). Furthermore the RF frequencies of this SPP are far below the cutoff at  $\omega_s \sim 1$  THz, and they thus travel with a group velocity close to  $c$ . The plasma wake currents, translating at  $c$  behind the laser pulse, thus co-propagate coherently with and steadily amplify the SPP surface wave at the leading edge of the plasma column. Simulations also show that the surface wave detaches efficiently from the end of the plasma column (end fire radiation [41, 42]) to become the forward directed pulse of RF.

The magnitude and spatial profile of the RF produced by this plasma wake surface wave model was found to accurately match far field broadband horn laboratory measurements [35]. In this work we revisit the theory with near-field D-dot measurements in the vicinity of the filamentation plasma. We find strong evidence of the Sommerfeld-Goubau SPPs predicted by the theory, with an excellent fit to a Hankel function radial profile and the  $r_{\text{outer}}$  length scale. We have also detected a longitudinal frequency drift in the SPPs that closely matches new axisymmetric Drude simulations, and new theoretical derivations for the phase velocity and resistive attenuation length scales. The measurement and characterization of these surface waves thus provides a new window into the physics of filamentation plasmas and for chirped pulse laser science in general.

## THEORY

The theory developed in [35] was developed through exploratory simulations at a variety of length scales, and then simplified into analytic approximations. Small scale PIC simulations that resolve the 800 nm wavelength and make use of the ionization rate  $\mathcal{W}$  given in [16] reproduce the electron velocity distributions given in [29] for linearly and circularly polarized laser pulses (and the large net transverse current for two color systems [43]). In the simplest PIC simulations the electrons are only accelerated by the remainder of the laser pulse, which yields the highest residual velocities for electrons born with instantaneous  $|E| = 0$ , but one can also include interactions with the parent ion which leads to additional heating (see also [44]).

We then perform larger PIC simulations of transverse slices of this plasma column where the initial electron velocities are set by the previous simulation. With 50 mJ of energy, the 50 fs pulses are in the multifilamentary regime [45], and we approximate the bundle of filament plasmas as one larger plasma column with radius  $r_{\text{pl}} = 500 \mu\text{m}$ . At atmospheric pressure the tail of the distribution is at about  $K_{\text{tail}} = 4 \text{ eV}$ , and with an electron-neutral collision frequency  $\nu$  of 5 THz these diffuse out to roughly  $r_{\Delta} = 30 \mu\text{m}$  over 100 ps, with an effective late time diffusion velocity of  $v_{\text{eff}} = 7 \times 10^4 \text{ m/s}$ . An analytic approximation for the radial current density  $J_r$  is given by:  $J_r = \epsilon_0 v_{\text{eff}} K_{\text{tail}} / r_{\Delta}^2$ , which is about 3000 A/m<sup>2</sup> at 10 GHz.

The presence of this broadband radial current pulse  $J_r$  on the outer boundary of the plasma column was found to excite a broadband SPP in axisymmetric Drude simulations [35]; Fig. 1 shows an updated simulation. This surface wave is well approximated by the transverse magnetic Sommerfeld-Goubau solution [46–51]. At a particular angular frequency  $\omega$  the radial component of the electric field  $E_r$  outside of the plasma is given by:

$$E_r(r, z, t) = -\frac{\pi r_{\text{pl}} E_0}{2r_{\text{outer}}} e^{i(\omega t - hz)} H_1^{(1)}(\gamma_{\text{air}} r), \quad (1)$$

where  $E_0$  is the amplitude of the wave at the surface of the plasma at  $r_{\text{pl}}$  (about  $10^4 \text{ V/m}$  at atmospheric pressure), the external  $\gamma_{\text{air}}$  is given by  $\gamma_{\text{air}}^2 = k_0^2 \epsilon_{\text{air}} - h^2$ , with  $\epsilon_{\text{air}} = \epsilon_{\text{air}} / \epsilon_0$ , free space wave number  $k_0 = \omega/c$ , complex wavenumber  $h$  which encodes both the SPP wavelength and attenuation length scale ( $L_{\text{decay}} = 1/\text{Im}(h)$ ), and  $H_1^{(1)}$  is a Hankel function of the first kind with order 1, with outer length scale  $r_{\text{outer}} = 1/|\gamma_{\text{air}}|$ . For radii  $\hat{r}$  between  $r_{\text{pl}}$  and  $r_{\text{outer}}$  the Hankel function is approximately  $H_1^{(1)} \simeq -2r_{\text{outer}}/(\pi r)$ , and for radii larger than  $r_{\text{outer}}$  it transitions to falling off exponentially: we fit the experimental D-dot data at a variety of frequency bands and radii to this predicted profile.

The  $r_{\text{outer}}$  length scale depends on  $h$ , which is found by matching the internal  $E_z$  and  $H_\phi$  fields (having  $J_0$  and  $J_1$

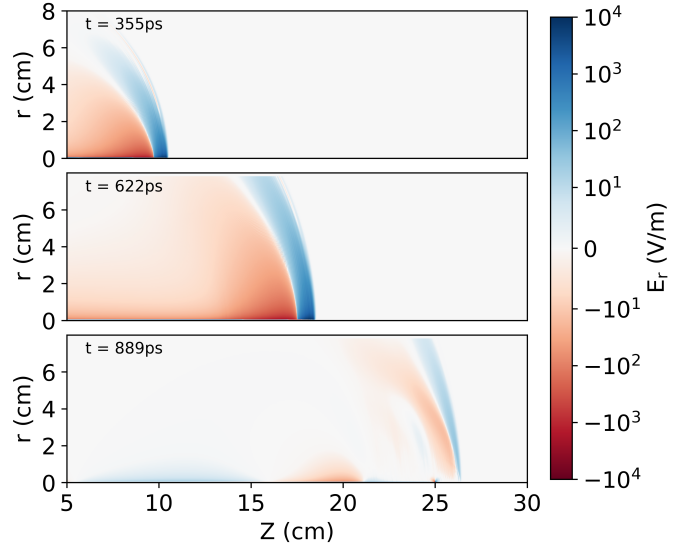


FIG. 1. Log plots of  $E_r$  for an axisymmetric Drude electromagnetic simulation at 3 points in time, with the SW near  $z = 10 \text{ cm}$  and  $z = 18 \text{ cm}$  at the top and middle, and free RF radiation shortly after detachment from the 25 cm plasma column on the bottom. The plasma column has a central number density of  $n_e = 10^{23} \text{ m}^{-3}$ , and has been given a  $\sin^2$  envelope in the  $\hat{z}$  direction (inspired by [52]), which causes the SW to both decay and smoothly detach over the final 5 cm with minimal upstream reflection (in contrast to the substantial reflection seen in previous uniform  $\hat{z}$  density simulations [35]).

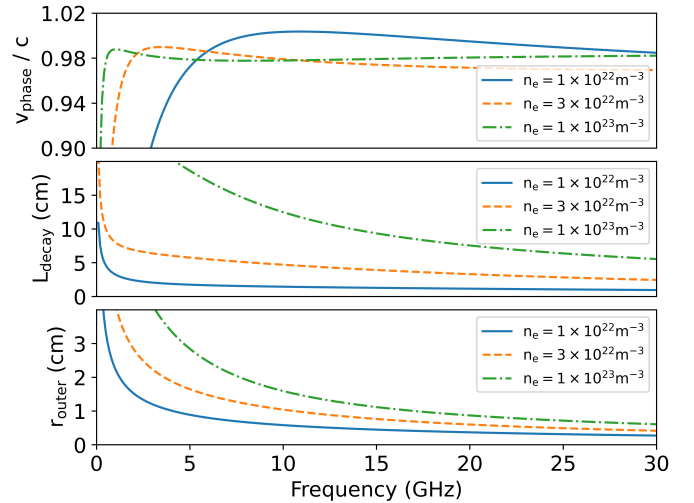


FIG. 2. Plots of the phase velocity, decay length, and outer length scale as a function of SPP frequency as calculated by (4), for a plasma column with radius  $r_{\text{pl}} = 0.5 \text{ mm}$ , collision frequency  $\nu = 5 \text{ THz}$ , and density  $n_e$  ranging from  $10^{22}$  to  $10^{23} \text{ m}^{-3}$ . The phase velocity slowly climbs towards  $c$  as the frequency decreases (as for planar SPPs), and then plunges when the skin depth becomes comparable to  $r_{\text{pl}}$ .  $L_{\text{decay}}$  and  $r_{\text{outer}}$  both increase for lower frequencies, with  $L_{\text{decay}}$  falling rapidly with decreasing  $n_e$ , and  $r_{\text{outer}}$  more slowly.

Bessel function dependences respectively) to the external fields (described by  $H_0^{(1)}$  and  $H_1^{(1)}$  Hankel functions) at the plasma column outer radius  $r_{\text{pl}}$ :

$$\frac{\gamma_{\text{air}} H_0^{(1)}(\gamma_{\text{air}} r_{\text{pl}})}{\varepsilon_{\text{air}} H_1^{(1)}(\gamma_{\text{air}} r_{\text{pl}})} = \frac{\gamma_{\text{pl}} J_0(\gamma_{\text{pl}} r_{\text{pl}})}{\varepsilon_{\text{pl}} J_1(\gamma_{\text{pl}} r_{\text{pl}})}, \quad (2)$$

with  $\gamma_{\text{pl}}^2 = k_0^2 \varepsilon_{\text{pl}} - h^2$  and relative plasma permittivity  $\varepsilon_{\text{pl}}$  [49] (and setting  $\varepsilon_{\text{air}} = 1$  from here on).

Sommerfeld originally solved (2) by using asymptotic approximations for the Bessel and Hankel functions and then developing an iterative method [46] to find  $h$ , and recent work has shown that those approximations can also yield a direct solution via the Lambert  $W$  function [53, 54]. We used this direct Lambert  $W$  method to estimate  $h$  in [35], but to get more accurate values for this work we have dropped the approximations and switched to an iterative method that uses the full Bessel and Hankel functions (see [49]). In particular, we include both the low and high frequency terms in the plasma permittivity:

$$\varepsilon_{\text{pl}}(\omega) = 1 + \frac{\omega_{\text{pl}}^2}{i\omega\nu - \omega^2}, \quad (3)$$

since  $\omega_{\text{pl}}$  is not too much smaller than  $\sigma_{\text{DC}} = \varepsilon_0 \omega_{\text{pl}}^2 / \nu$ . At lower frequencies the skin depth  $\sqrt{2/\sigma_{\text{DC}} \mu \omega}$  can be comparable to the plasma radius  $r_{\text{pl}}$ , and so we also do not use the  $J_0/J_1 = i$  approximation. We thus rearrange the full (2) equation to give the  $N + 1$  iteration for  $\gamma_{\text{air}}$ :

$$\gamma_{\text{air}}^{N+1} = \frac{\gamma_{\text{pl}}^N H_1^{(1)}(\gamma_{\text{air}}^N r_{\text{pl}}) J_0(\gamma_{\text{pl}}^N r_{\text{pl}})}{\varepsilon_{\text{pl}} H_0^{(1)}(\gamma_{\text{air}}^N r_{\text{pl}}) J_1(\gamma_{\text{pl}}^N r_{\text{pl}})}, \quad (4)$$

with  $\gamma_{\text{pl}}^N = \sqrt{(\gamma_{\text{air}}^N)^2 + (\varepsilon_{\text{air}}(\omega) - 1)k_0^2}$ , an initial  $N = 1$  guess of  $\gamma_{\text{air}}^{N=1} = 0.5k_0$ , and  $h = \sqrt{k_0^2 - \gamma_{\text{air}}^2}$  once the iteration has converged (typically 10-30 steps - see [54] for further discussion on convergence criteria). For a plasma with an estimated values  $r_{\text{pl}} = 500 \mu\text{m}$ ,  $\nu \sim 5 \text{ THz}$ ,  $n_e \sim 3 \times 10^{22} \text{ m}^{-3}$  (giving  $\sigma_{\text{DC}} \sim 170 \text{ S/m}$ ), and a surface wave frequency of 10 GHz, (4) yields  $h \simeq 214 + 21i$ , which gives  $r_{\text{outer}} \sim 1.0 \text{ cm}$ , and a longitudinal  $1/e$  attenuation length scale of  $L_{\text{decay}} \sim 4.7 \text{ cm}$ . We note that with longer laser pulses the electron density  $n_e$  can grow much higher, especially as collisional heating and ionization become important [55], which leads to higher conductivity, a larger plasma radius and better surface wave propagation and growth.

We base our theory on the Sommerfeld-Goubau solution (1), but additional dynamics occur in the surface wave simulations (see Fig. 1) that are not easily captured by analytic approximations. The analytic solutions assume a Heaviside step function profile in the conductor electron density, which is a good approximation for optical SPPs on metal substrates, but less so for the boundaries of plasmas. However, in simulation when we switch

from a step function to a radial electron density gradient at the outer boundary of the plasma we get qualitatively similar SPPs, with the amplitude  $E_0$  of these gradient-boundary waves somewhat suppressed, and the spatial wave length moderately increased.

We also observe that the plasma wake radial current directly excites some free radiation in addition to the surface wave: this lower amplitude free radiation can be seen to slowly pull ahead of the surface wave over long simulations (and can be seen in Fig. 1 given the log scale). We suspect that the D-dot probe is also detecting this prompt free radiation in the experiments.

The original simulations performed in [35] used plasma columns with constant density in the longitudinal  $\hat{z}$  direction, but given the experimental measurements in [52] we have switched to a more realistic tapered  $n_e(z) = n_{e,\text{max}} \sin^2(\pi z/L_{\text{pl}})$  profile, with low plasma densities at the beginning and end of the column. The use of this tapered profile results in modulation of the SPP amplitude that closely mirrors the near field experimental data. It also helps to explain the absence of higher frequency far field RF in experiments such as [31] (given the presence of high amplitude, high frequency content in  $J_r$ ), as higher frequency SPPs are more strongly attenuated in low density regions (see Fig. 2). We also find a frequency dependent drift in the simulated SPP peak amplitudes that closely matches the longitudinal D-dot measurements. We note that the dispersion of SPPs in a cylindrical geometry is more complex than on a plane, with the group velocity of low frequency waves dropping rapidly instead of converging to  $c$  [50, 51], as can be seen in Fig. 2. On a filamentation plasma where Kerr focusing and plasma defocusing can compete to form islands of high density plasma this can cause the lowest frequency SPPs to become trapped on the high density islands.

## EXPERIMENTATION

To investigate the near-field region of a femtosecond plasma, an 800 nm wavelength 50 mJ laser was used with a 50 fs pulse duration and a 10 Hz repetition rate. Plasma formed near the geometric focal point of a 3 m focusing optic (leading to somewhat higher  $n_e$ ). Fig. 3 shows the visible fluorescence of the plasma column which spans approximately 18 cm across the top of an optical bench.

A Prodyn FD-5C2 D-dot probe (bandwidth of 2-40 GHz) was used to measure the electric field generated by the plasma column. From preliminary experiments, the strongest signal was received by the D-dot probe when placing the probe tip normal to the direction of plasma propagation (see Fig. 3). The probe was mounted to a 2 inch micrometer stage (movable in the  $\hat{r}$  direction) in the same plane as the plasma column. The stage was attached to two consecutive 33 inch optical rails mounted along the direction of propagation. This allowed for the

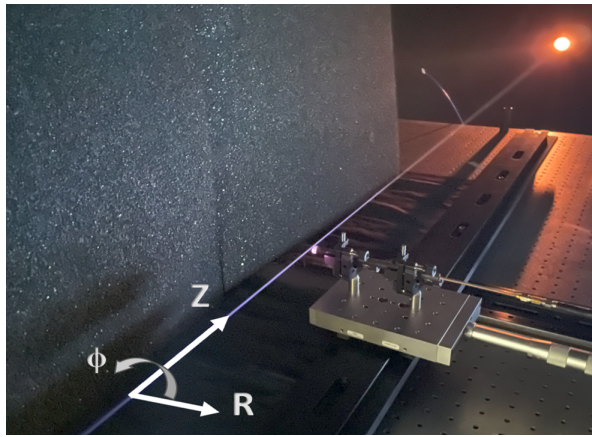


FIG. 3. The 800nm laser plasma column was generated with the aid of lens assisted filamentation to conserve laboratory space. The D-dot probe is located on an  $\hat{r}$  direction translation stage and is swept in the  $\hat{z}$  direction using an optical rail.

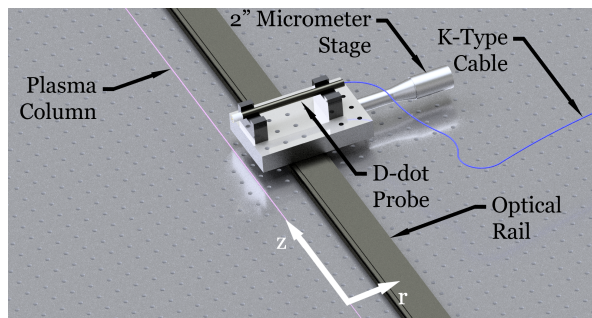


FIG. 4. The above rendering shows the components utilized during experimentation. The Prodyn FD-5C2 D-dot probe is mounted atop a 2 inch micrometer stage which moves along the  $\hat{r}$  axis. Additionally, the stage is mounted to a 72.5 inch optical rail; this allows for movement along the  $\hat{z}$  axis. The plasma column propagates along the positive  $\hat{z}$  axis as shown above. K-type coaxial cable was used to connect to the oscilloscope, and microwave foam was placed parallel to the plasma to reduce signal reflections.

probe to be positioned both along the  $\hat{z}$  direction of the plasma and at various radius locations in the  $\hat{r}$  direction. By mounting the probe in such a configuration, the plasma column was able to be examined in increments of  $1/16$  inch in the  $\hat{z}$  direction and  $0.001$  mm in the  $\hat{r}$  direction. The laser was carefully aligned through two irises to ensure the D-dot probe would remain at a fixed radius from the plasma column while moving along the  $z$  axis. An index card flush with the D-dot was periodically ablated by the plasma column at various  $\hat{z}$  distances to confirm the distance between the probe tip and the plasma column remained constant. The experimental setup is depicted by the rendering in Fig. 4.

Data was collected by selecting a stationary radius  $r$  and longitudinally scanning in the  $\hat{z}$  direction with the D-dot probe;  $r$  values of 0.5, 0.75, 1.0, 1.5, and 2.0 cm were

probed at 28 locations along the  $\hat{z}$  axis ranging from 248.9 cm to 320.0 cm from the focusing optic. Steps along the  $\hat{z}$  axis were taken in 2.54 cm increments. Additionally, radial data was collected at the fixed longitude location of highest signal ( $z = 294.6$  cm) for 19 evenly spaced radii between 0.25 cm and 5.0 cm from the plasma surface (note that we later shift our  $z$  coordinate system to begin with of plasma formation, so that  $z = 295$  cm becomes  $z = 18$  cm). For both experiments laser output energy was measured at the beginning and end of each test. The signal received by the D-dot probe was digitally captured using a Tektronix DP077002SX 33 GHz oscilloscope which limited the upper frequency limit of the measurements. The D-dot probe was connected to the oscilloscope using a K-type (40 GHz) cable.

## RESULTS

After collecting the raw data in the Tektronics digital oscilloscope, a Fast Fourier Transform (FFT) was applied to the time dependent signals to obtain the frequency content within the 2-33 GHz microwave regime. The noise floor from the laboratory environment was also recorded, and the resulting noise FFT subtracted from the signal FFTs. We note that developing an accurate, frequency dependent calibration of the D-dot probe (see e.g. [31]) is non-trivial, and we leave it for future work. As the D-dot amplitudes are uncalibrated, the measured values of the electric fields at different frequencies should only be considered in a relative context.

Fig. 5 shows the FFTs taken at 4 radial separations ranging from  $r = 0.5$  cm to  $r = 1.5$  cm, taken near the peak at  $z = 18$  cm, as well as the noise signal recorded when the laser pulse is blocked at the focusing lens and no plasma forms (note that each curve is the average of 50 individual shots). Although the data is uncalibrated the ultra-broadband nature of the near field waves is clear, (as can also be seen in the original time series data), and the overall profile resembles the far field RF recorded in [31].

We next average the radial FFT data over large frequency bins so that we can compare with theory. In general the radial fall off is very well fit by the expected Hankel function dependence in (1), and is much better than naive polynomial fits. Fig 6 shows the single best fit that occurs at 14 GHz (which is also about the frequency of largest signal - see Fig. 5), with an  $R^2$  value of 0.9993. All of the frequency bins are best fit by the Hankel function dependence, with typical  $R^2$  values of about 0.99. The radial dependence of simulated SWs (see Fig. 1) is also very well fit by a Hankel function, with  $R^2$  values better than 0.9999.

We note that the Hankel function fit underpredicts the measured data starting at about 2.5 cm in Fig. 6, and this trend is seen in the other frequency bins. In sim-

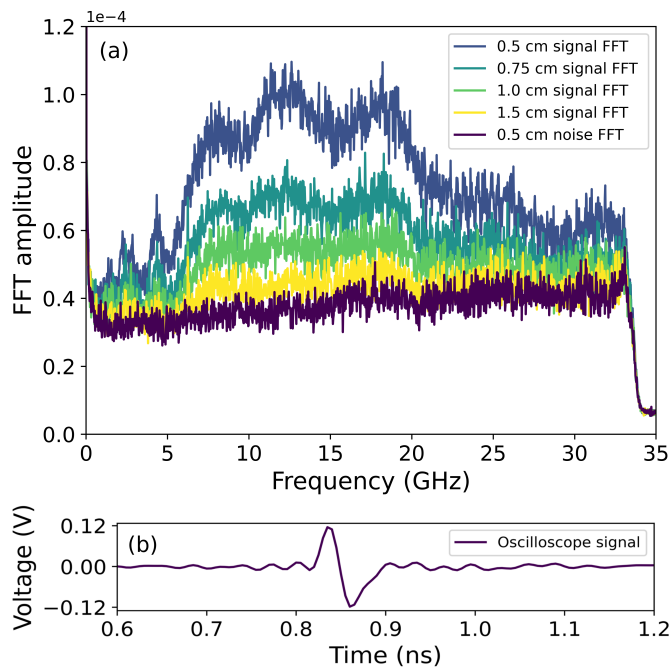


FIG. 5. (a) FFTs of measured electron field strength measured at  $z = 18$  cm (near the peak) for radial separations ranging from 0.5 cm to 1.5 cm, along with the measured noise spectrum taken when no filamentation is occurring. The near field D-dot probe has not been calibrated for this experiment, but the broadband signal resembles the far field data taken in [31]. In all frequency bins the amplitude of the signal above the noise floor falls off rapidly with increasing distance. (b) An example time domain signal recorded by the oscilloscope at a separation of 0.5 cm.

ulation some free radiation is also excited by the radial  $J_r$  currents, and the amplitude of this radiation will fall off more slowly than the Hankel function at large radius ( $r > r_{\text{outer}}$ ). We thus suspect that we are also detecting this free radiation, although the overall amplitude of the measured signal is small at this larger radius.

Given the Hankel function fits we can also extract the fit values for the outer length scale  $r_{\text{outer}}$  and compare with theory. We find that the experimental  $r_{\text{outer}}$  values match well with an electron density of  $n_e = 3 \times 10^{22} \text{ m}^{-3}$  (see Fig. 2), with an experimental fit  $r_{\text{outer}} = 0.75$  cm at 15 GHz being close to the theory value given by (4). However the slope of the experimental values as a function of frequency is lower than the theoretical curve, as can be seen in Fig. 6.

We next consider the longitudinal variation in the measured D-dot signal. Fig. 7 shows the amplitude as a function of  $z$  for 5 frequency bins ranging from 5 GHz to 25 GHz, as measured at  $r = 2.5$  mm in both the experimental and Drude simulation data (see Fig. 1). As a D-dot calibration is not available the different frequencies have all been normalized to 1 for comparison purposes. We

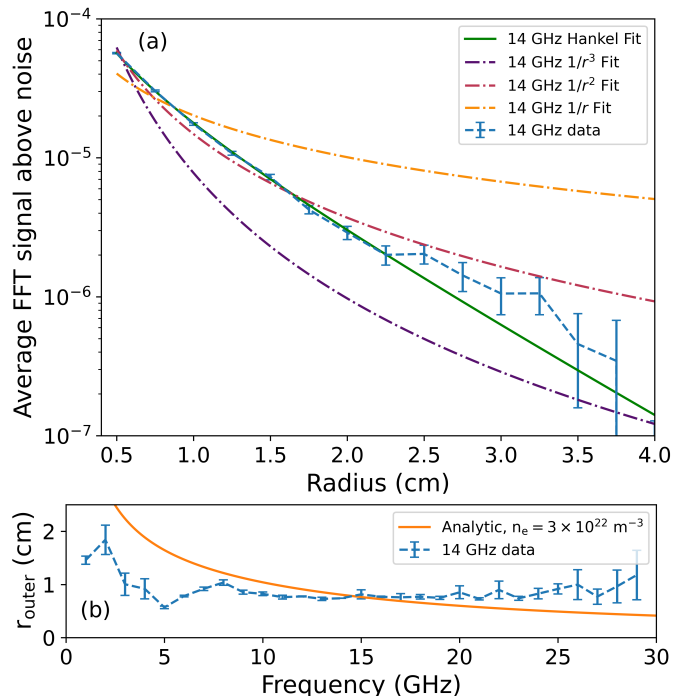


FIG. 6. (a) Log scale plot of the 14 GHz bin data (collected at  $z = 18$  cm) for radii between  $r = 0.25$  cm and 3.75 cm. The radial data in all frequency bins is well fit by the expected Hankel function dependence (1), with typical  $R^2$  values of 0.99, and the 14 GHz bin yields the best fit, with  $R^2 = 0.9993$ . Visually the Hankel fit is very good out to a distance of about 2 cm, much better than the naive  $1/r$ ,  $1/r^2$ , and  $1/r^3$  profiles, and then it slightly underpredicts the measured signal at larger radii. We suspect that this is due to the presence of free radiation, in addition to the bound SPP wave, which the simulations also generically predict to be excited (see Fig. 1). (b) Comparison of the  $r_{\text{outer}}$  values from Hankel function fits as a function of frequency, compared to the analytic expectation from (4) with an electron density of  $n_e = 3 \times 10^{22} \text{ m}^{-3}$ . The overall magnitude is quite close, although the slope of the experimental data is flatter than the theoretical expectation.

note that there is a consistent drift of the peaks of the different frequencies to larger  $z$  as the frequency decreases in both the experimental data and in the simulations.

This longitudinal drift towards lower frequencies is consistent with the theoretical expectations shown in Fig. 2: from higher frequencies down to about 5 GHz the phase velocity of the SPPs is approaching  $c$ , and thus the lower frequency surface waves have better phase coherence with the  $J_r$  current source. The lower frequency waves also decay more slowly, helping them to build to a later peak. At even lower frequencies below 5 GHz the phase velocity rapidly drops (depending sensitively on the electron density), and the waves no longer co-propagate efficiently with  $J_r$ , and the amplitude of the SPPs falls off quickly. We note that the experimental curves become much noisier below 5 GHz, which we suspect is due to density fluctuations along the plasma col-

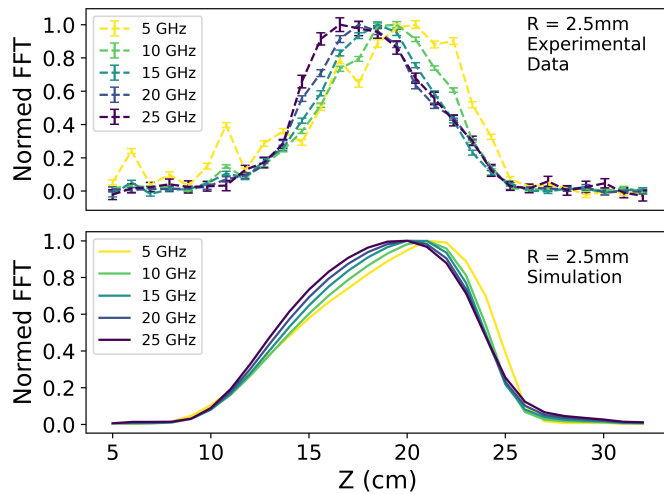


FIG. 7. Normalized traces of measured electric field strength in 5 different frequency bins as a function of longitudinal position  $z$ , for both the experimental data and the corresponding simulation shown in Fig. 1. In both cases the higher frequency components of the wave reach their maximums at earlier  $\hat{z}$  positions, and the lowest frequencies reach their maximums last. The experimental data also becomes successively more noisy at lower frequencies, which we suspect is due to a combination of phase velocity drop off at low frequencies, and focusing and defocusing effects modulating the plasma column density.

umn due to focusing and de-focusing effects, and which the lower frequencies are more sensitive to. At the larger  $z$  values towards the end of the plasma column the electron density  $n_e$  drops off, which causes the waves to both decay more quickly and detach from the plasma column, leading to a collapse of the signal.

Inspired by exploratory simulations we argued in [35] that SPPs are both generated during femtosecond filamentation, and grow in strength due to coherent copropagation near the speed of light with the plasma wake currents that excite them along the leading edge of the plasma column. In this paper we present new near field data that is in excellent agreement with this theory. We find that the radial profile of the D-dot measurements is in very good agreement with the expected Hankel function dependence from the Sommerfeld-Goubau solution, and the characteristic outer length scale is well matched by a plasma with density  $n_e = 3 \times 10^{22} \text{ m}^{-3}$ . In turn the longitudinal frequency drift data seen in the data is in good agreement with both theoretical expectations for the phase velocity and decay length (4), and with new simulations (Fig. 1) that include variations in plasma density [52]. The near field measurement of these surface waves thus provides a powerful new scientific tool for chirped pulse filamentation research.

*Acknowledgments.* The authors thank the Air Force Office of Scientific Research (AFOSR) for support via Laboratory Task No. FA9550-24RDCOR002. This work

was supported in part by high-performance computer time and resources from the DoD High Performance Computing Modernization Program. Approved for public release; distribution is unlimited. Public Affairs release approval No. AFRL-2024-6758.

- [1] D Kordeweg and G de Vries, “On the change of form of long waves advancing in a rectangular channel, and a new type of long stationary wave,” *Phil. Mag* **39**, 422–443 (1895).
- [2] Norman J Zabusky and Martin D Kruskal, “Interaction of “solitons” in a collisionless plasma and the recurrence of initial states,” *Physical review letters* **15**, 240 (1965).
- [3] Mark J Ablowitz and Harvey Segur, “On the evolution of packets of water waves,” *Journal of Fluid Mechanics* **92**, 691–715 (1979).
- [4] Lord Rayleigh, “On waves propagated along the plane surface of an elastic solid,” *Proceedings of the London mathematical Society* **1**, 4–11 (1885).
- [5] Augustus Edward Hough Love, *Some Problems of Geodynamics: Being an Essay to which the Adams Prize in the University of Cambridge was Adjudged in 1911* (University Press, 1911).
- [6] Per Delsing, Andrew N Cleland, Martin JA Schuetz, Johannes Knörzer, Géza Giedke, J Ignacio Cirac, Kartik Srinivasan, Marcelo Wu, Krishna Coimbatore Balram, Christopher Bäuerle, *et al.*, “The 2019 surface acoustic waves roadmap,” *Journal of Physics D: Applied Physics* **52**, 353001 (2019).
- [7] Michel I D’yakonov, “New type of electromagnetic wave propagating at an interface,” *Sov. Phys. JETP* **67**, 714–716 (1988).
- [8] Pochi Yeh, Amnon Yariv, and Chi-Shain Hong, “Electromagnetic propagation in periodic stratified media. i. general theory,” *JOSA* **67**, 423–438 (1977).
- [9] John A Polo Jr and Akhlesh Lakhtakia, “Surface electromagnetic waves: a review,” *Laser & Photonics Reviews* **5**, 234–246 (2011).
- [10] Osamu Takayama, AA Bogdanov, and Andrei V Lavrinenko, “Photonic surface waves on metamaterial interfaces,” *Journal of Physics: Condensed Matter* **29**, 463001 (2017).
- [11] Saman Jahani and Zubin Jacob, “All-dielectric metamaterials,” *Nature nanotechnology* **11**, 23–36 (2016).
- [12] Rufus H Ritchie, “Plasma losses by fast electrons in thin films,” *Physical review* **106**, 874 (1957).
- [13] JM Pitarke, VM Silkin, EV Chulkov, and PM Echenique, “Theory of surface plasmons and surface-plasmon polaritons,” *Reports on progress in physics* **70**, 1 (2006).
- [14] Andreas Otto, “Excitation of nonradiative surface plasma waves in silver by the method of frustrated total reflection,” *Zeitschrift für Physik A Hadrons and nuclei* **216**, 398–410 (1968).
- [15] Erwin Kretschmann and Heinz Raether, “Radiative decay of non radiative surface plasmons excited by light,” *Zeitschrift für Naturforschung A* **23**, 2135–2136 (1968).
- [16] SV Popruzhenko, VD Mur, VS Popov, and D Bauer, “Strong field ionization rate for arbitrary laser frequencies,” *Physical review letters* **101**, 193003 (2008).

- [17] A Braun, G Korn, X Liu, D Du, J Squier, and G Mourou, “Self-channeling of high-peak-power femtosecond laser pulses in air,” .
- [18] Francis Théberge, Weiwei Liu, Patrick Tr Simard, Andreas Becker, and See Leang Chin, “Plasma density inside a femtosecond laser filament in air: Strong dependence on external focusing,” *Physical Review E* **74**, 036406 (2006).
- [19] Arnaud Couairon and André Mysyrowicz, “Femtosecond filamentation in transparent media,” *Physics reports* **441**, 47–189 (2007).
- [20] Jérôme Kasparian and Jean-Pierre Wolf, “Physics and applications of atmospheric nonlinear optics and filamentation,” *Optics express* **16**, 466–493 (2008).
- [21] SL Chin, T J Wang, C Marceau, J Wu, JS Liu, O Kosareva, N Panov, YP Chen, J F Daigle, S Yuan, *et al.*, “Advances in intense femtosecond laser filamentation in air,” *Laser Physics* **22**, 1–53 (2012).
- [22] Zhaxylyk A Kudyshev, Martin C Richardson, and Natalia M Litchinitser, “Virtual hyperbolic metamaterials for manipulating radar signals in air,” *Nature communications* **4**, 2557 (2013).
- [23] Shermineh Rostami, Michael Chini, Khan Lim, John P Palastro, Magali Durand, Jean-Claude Diels, Ladan Aris- sian, Matthieu Baudelet, and Martin Richardson, “Dramatic enhancement of supercontinuum generation in elliptically-polarized laser filaments,” *Scientific Reports* **6**, 20363 (2016).
- [24] J Kasparian and J-P Wolf, “Ultrafast laser spectroscopy and control of atmospheric aerosols,” *Physical Chemistry Chemical Physics* **14**, 9291–9300 (2012).
- [25] Chung-Chieh Cheng, Ewan M Wright, and Jerome V Moloney, “Generation of electromagnetic pulses from plasma channels induced by femtosecond light strings,” *Physical Review Letters* **87**, 213001 (2001).
- [26] Phillip Sprangle, JR Penano, Bahman Hafizi, and CA Kapetanacos, “Ultrashort laser pulses and electromagnetic pulse generation in air and on dielectric surfaces,” *Physical Review E* **69**, 066415 (2004).
- [27] Ciro D’Amico, Aurélien Houard, Michel Franco, Bernard Prade, André Mysyrowicz, Arnaud Couairon, and VT Tikhonchuk, “Conical forward thz emission from femtosecond-laser-beam filamentation in air,” *Physical review letters* **98**, 235002 (2007).
- [28] CD Amico, Aurélien Houard, Selcuk Akturk, Yi Liu, J Le Bloas, Michel Franco, Bernard Prade, Arnaud Couairon, VT Tikhonchuk, and André Mysyrowicz, “Forward thz radiation emission by femtosecond filamentation in gases: theory and experiment,” *New Journal of Physics* **10**, 013015 (2008).
- [29] Bing Zhou, Aurélien Houard, Yi Liu, Bernard Prade, André Mysyrowicz, Arnaud Couairon, Patrick Mora, Christopher Smeenk, Ladan Aris- sian, and Paul Corkum, “Measurement and control of plasma oscillations in femtosecond filaments,” *Physical review letters* **106**, 255002 (2011).
- [30] Benjamin Forestier, Aurélien Houard, Magali Durand, Yves-Bernard André, Bernard Prade, J-Y Dauvignac, Franck Perret, Ch Pichot, Michel Pellet, and André Mysyrowicz, “Radiofrequency conical emission from femtosecond filaments in air,” *Applied Physics Letters* **96**, 141111 (2010).
- [31] Alexander Englesbe, Jennifer Elle, Remington Reid, Adrian Lucero, Hugh Pohle, Matthew Domonkos, Serge Kalmykov, Karl Krushelnick, and Andreas Schmitt-Sody, “Gas pressure dependence of microwave pulses generated by laser-produced filament plasmas,” *Optics Letters* **43**, 4953–4956 (2018).
- [32] A Janicek, E Thornton, T Garrett, A Englesbe, J Elle, and A Schmitt-Sody, “Length dependence on broadband microwave emission from laser-generated plasmas,” *IEEE Transactions on Plasma Science* **48**, 1979–1983 (2020).
- [33] AV Mitrofanov, DA Sidorov-Biryukov, MM Nazarov, AA Voronin, MV Rozhko, AB Fedotov, and AM Zheltikov, “Coherently enhanced microwave pulses from midinfrared-driven laser plasmas,” *Optics Letters* **46**, 1081–1084 (2021).
- [34] Alexander Englesbe, Jennifer Elle, Robert Schwartz, Travis Garrett, Daniel Woodbury, Dogeun Jang, Ki-Yong Kim, Howard Milchberg, Remington Reid, Adrian Lucero, *et al.*, “Ultrabroadband microwave radiation from near-and mid-infrared laser-produced plasmas in air,” *Physical Review A* **104**, 013107 (2021).
- [35] Travis Garrett, Jennifer Elle, Michael White, Remington Reid, Alexander Englesbe, Ryan Phillips, Peter Mardahl, Erin Thornton, James Wymer, Anna Janicek, *et al.*, “Generation of radio frequency radiation by femtosecond filaments,” *Physical Review E* **104**, L063201 (2021).
- [36] Charles K Birdsall and A Bruce Langdon, *Plasma physics via computer simulation* (CRC press, 2004).
- [37] Robert E Peterkin and John W Luginsland, “A virtual prototyping environment for directed-energy concepts,” *Computing in Science & Engineering* **4**, 42–49 (2002).
- [38] M Okoniewski, M Mrozowski, and MA Stuchly, “Simple treatment of multi-term dispersion in fdtd,” *IEEE Microwave and Guided Wave Letters* **7**, 121–123 (1997).
- [39] Fernando L Teixeira, “Time-domain finite-difference and finite-element methods for maxwell equations in complex media,” *IEEE Transactions on Antennas and Propagation* **56**, 2150–2166 (2008).
- [40] Jianing Chen, Michela Badioli, Pablo Alonso-González, Sukosin Thongrattanasiri, Florian Huth, Johann Osmond, Marko Spasenović, Alba Centeno, Amaia Pesquera, Philippe Godignon, *et al.*, “Optical nano-imaging of gate-tunable graphene plasmons,” *Nature* **487**, 77–81 (2012).
- [41] JB Andersen, “Radiation from surface-wave antennas,” *Electronics Letters* **3**, 251–252 (1967).
- [42] GI Stegeman, RF Wallis, and AA Maradudin, “Excitation of surface polaritons by end-fire coupling,” *Optics letters* **8**, 386–388 (1983).
- [43] Ki-Yong Kim, James H Glow- nia, Antoinette J Taylor, and George Rodriguez, “Terahertz emission from ultrafast ionizing air in symmetry-broken laser fields,” *Optics express* **15**, 4577–4584 (2007).
- [44] Paul B Corkum, “Plasma perspective on strong field multiphoton ionization,” *Physical review letters* **71**, 1994 (1993).
- [45] L Bergé, S Skupin, F Lederer, G Méjean, J Yu, J Kasparian, E Salmon, JP Wolf, M Rodriguez, L Wöste, *et al.*, “Multiple filamentation of terawatt laser pulses in air,” *Physical Review Letters* **92**, 225002 (2004).
- [46] Arnold Sommerfeld, “Ueber die fortpflanzung elektrodynamischer wellen längs eines drahtes,” *Annalen der Physik* **303**, 233–290 (1899).
- [47] Georg Goubau, “Surface waves and their application to transmission lines,” *Journal of Applied Physics* **21**, 1119–1128 (1950).

- [48] Julius Adams Stratton, *Electromagnetic theory*, Vol. 33 (John Wiley & Sons, 2007).
- [49] Sophocles J Orfanidis, “Electromagnetic waves and antennas,” (2002).
- [50] CA Pfeiffer, EN Economou, and KL Ngai, “Surface polaritons in a circularly cylindrical interface: surface plasmons,” *Physical review B* **10**, 3038 (1974).
- [51] Kanglin Wang and Daniel M Mittleman, “Dispersion of surface plasmon polaritons on metal wires in the terahertz frequency range,” *Physical Review Letters* **96**, 157401 (2006).
- [52] Anna M Janicek, “Measuring energy deposition from a laser induced plasma in air which generates broadband microwave radiation,” (2023).
- [53] Denis Jaisson, “Simple formula for the wave number of the goubau line,” *Electromagnetics* **34**, 85–91 (2014).
- [54] J Ricardo G Mendonça, “Electromagnetic surface wave propagation in a metallic wire and the lambert w function,” *American Journal of Physics* **87**, 476–484 (2019).
- [55] Erin Thornton, Travis Garrett, and Jennifer Elle, “Boosting radio frequency radiation with collisional processes in picosecond laser filamentation,” *Physics of Plasmas* **31**, 050702 (2024).